In-Situ Reconstruction-Regulated Fe-Doped $Ni(OH)_2$ for Glucose Oxidation Electrocatalytic-Enhanced Seawater Electrolysis

Yan Sun [ab], Yifei Su [a], Zhibin Liang [a], Yuexia Li [a], Hairui Guo [b], Xin Jiao[a]*

E-mail: (jiaoxin@sxct.edu.cn Prof. X. Jiao).

[a]College of Materials Engineering, Shanxi College of Technology, Shuozhou 036000, P.R. China

[b]Tianjin Key Laboratory of Advanced Functional Porous Materials, Institute for New Energy Materials & Low-Carbon Technologies, School of Materials Science and Engineering, Tianjin University of Technology, Tianjin 300384, P.R. China

1. Experiment Section

1.1. Chemical and Materials

Nickel foam (thickness 1.6 mm) and Fumasep FAA-3-PK-130 anionic membrane were purchased from Suzhou Shuertai Industrial Technology Co., Ltd., China. Hydrochloric acid (HCl) was sourced from National Pharmaceutical Group Co., Ltd. Nickel(II) chloride hexahydrate ($NiCl_2·6H_2O$), iron(III) nitrate nonahydrate ($Fe(NO_3)_3·9H_2O$), hexamethylenetetramine, potassium hydroxide (KOH), glucose ($C_6H_{12}O_6$) were obtained from Sigma-Aldrich Corporation. All chemicals were of analytical grade and were used without further purification.

1.2. Synthesis of $Fe_xNi(OH)_2$@NF Catalysts

A 2×2 cm^2 piece of NF was ultrasonically treated sequentially in 3.0 M HCl for 30 min, ethanol for 10 min, and ultrapure water for 10 min to remove surface contaminants and oxide layers. Afterward, the NF was dried in an oven to yield the pretreated NF. $NiCl_2·6H_2O$ (0.85 mmol), $Fe(NO_3)_3·9H_2O$ (0.15 mmol), and hexamethylenetetramine (2 mmol) were weighed and dissolved in 18 mL of ultrapure

water. The mixture was magnetically stirred for 30 min to obtain a clear solution, which was then transferred into the 25 mL Teflon-lined autoclave. The pretreated NF was placed vertically against the inner wall of the autoclave. The autoclave was heated at 120 °C for 10 h. After cooling to room temperature, the NF coated with catalyst was removed, rinsed thoroughly with ultrapure water, and dried at 60 °C in an oven, yielding the $Fe_{0.15}Ni(OH)_2$@NF catalyst.

For comparison, catalysts with different Fe doping levels of $Fe_{0.05}Ni(OH)_2$@NF, $Fe_{0.10}Ni(OH)_2$@NF, $Fe_{0.20}Ni(OH)_2$@NF, and $Fe_{0.25}Ni(OH)_2$@NF were prepared using the same procedure but with 0.05, 0.10, 0.20, and 0.25 mmol of $Fe(NO_3)_3 \cdot 9H_2O$, respectively.

2. Materials characterization

The structures and morphologies of the prepared samples were characterized by X-ray diffraction (XRD, MiniFlex 600, Rigaku, Japan), scanning electron microscope (SEM, Verios 460L, USA) equipped with a LaB6 emission gun. The water droplet and underwater gas-bubble contact angle of the samples were recorded using KRüSS-DSA100 (Germany) contact angle meter. The Fe and Ni contents of as-prepared catalysts were quantified by inductively coupled plasma optical emission spectroscopy (ICP-OES, Thermo Scientific).

3. Electrochemical Measurements

3.1 HER and GOR electrochemical measurements

All the electrochemical measurements were conducted on a CORRESET CS350M electrochemical workstation in an H-type cell, separated by a Fumasep FAA-3-PK-130 anionic membrane, unless otherwise stated. The electrochemical studies utilized a conventional three-electrode configuration, with the as-synthesized catalyst on Ni foam (1.0 × 1.0 cm^2), Hg/HgO, and a graphite rod were used as the working electrode, reference, and counter electrode, respectively. Linear sweep voltammetry (LSV) curves were performed at a scan rate of 5 mV s^{-1} until the results

stabilized, with 85% iR compensation was applied to eliminate most ohmic drop while avoiding potential oscillation caused by over-compensation.[1, 2]

The Hg/HgO electrode was calibrated with respect to reversible hydrogen electrode (RHE) at 25°C. The calibration was performed in 1.0 M KOH electrolyte with a Pt wire as working electrode. CVs were run at a scan rate of 1 mV s^{-1}, and the average of the two potentials at which the current crossed zero was taken to be the thermodynamic potential for the hydrogen electrode reactions.[3] As shown in Fig. S1, the potential reported in our work were convert RHE according to the equation (1):

$$E_{vs.\ RHE} = E_{vs.\ Hg/HgO} + 0.93\ V \quad (S1)$$

Where $E_{vs.\ RHE}$ and $E_{vs.\ Hg/HgO}$ are the potentials against RHE and Hg/HgO, respectively.

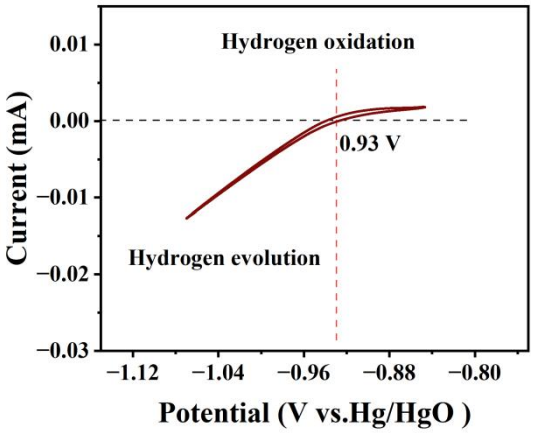

Fig. S1 The CV result of RHE calibration in 1.0 M KOH solution, $E_{vs.\ RHE} = E_{vs.\ Hg/HgO} + 0.93$ V.

The electrochemical double-layer capacitance (C_{dl}) was used to estimate the electrochemical surface area (ECSA) of the electrocatalyst. C_{dl} was obtained by CV method at various scanning rates (1, 3, 5, 7, 9, and 10 mV s^{-1}) in 1.0 M KOH containing 0.1 M glucose. In-situ EIS tests were conducted with a three-electrode system within a a frequency range of 10^{-1} to 10^{5} Hz with an AC amplitude of 10 mV.

3.2 Assembly and tests of the two-electrode electrolyzer

To measure the performances of the two-electrode electrolysis, the as-prepared catalysts were used as both anode and cathode. LSV curves were recorded at a scan rate of 5 mV s^{-1} in 1.0 M KOH with and without 0.1 M glucose. For the anion exchange membrane (AEM) flow electrolyzer, a Fumasep FAA-3-PK-130 anionic membrane was purchased from Suzhou Shengernuo Co., LTD. The membrane was sandwiched between the anode and cathode (effective electrode area: 1.0 × 1.0 cm^2). Electrolytes were fed into the AEM flow electrolyzer through pump (Flow rate: 10 mL min^{-1}) at 60 ℃. To minimize errors and uncertainties, the electrochemical performance test results were repeatedly verified. The stability test of the AEM flow electrolyzer was performed at a constant current density of 50 mA cm^{-2}, and both LSV curves and stability tests were recorded without iR compensation.

3.3 In Situ Raman spectra

In situ Raman spectra were carried out on a laser confocal Raman spectroscopy (HORIBA EVOLUTION, France). The electrolytic cell for in situ Raman Spectrum comprises a Teflon shell, quartz glass plate, Pt wire, and Ag/AgCl electrodes. All the electrochemical tests were carried out using the three-electrode configuration connected to an electrochemical workstation (CHI-660E). The counter electrode was a platinum wire for HER. The electrolyte is 1.0 M KOH with or without 0.1 M glucose for the GOR and OER testing.

3.4 Product Analysis of GOR

The concentrations of glucose and oxidation products were quantified by high-performance liquid chromatography (HPLC, Agilent 1260) equipped with a Biorad HPX-87H column. Glucose concentrations were determined using a refractive index (RI) detector, while oxidation products were measured using a UV detector operating at 210 nm. The mobile phase was 5 mM H_2SO_4 with a flow rate of 0.6 mL·min^{-1}. During the chronopotentiometric measurements, 50 μL of electrolyte was

extracted and subsequently diluted to 1 mL with 0.5 M H_2SO_4 aqueous solution. The injection volume was 1 μL, column temperature was maintained at 35°C, and analysis time was 20 min per sample. The faradaic efficiency (FE) of products was calculated using equation (2):

$$FE(\%) = \frac{\text{moles of product} \times n \times F}{\text{total charge passed}} \times 100\% \quad \text{(S2)}$$

where n is the electron transfer number (n = 2 for formate and gluconate)[4-6] and F is the Faraday constant (96485 $C \cdot mol^{-1}$).

4. Supplementary Results

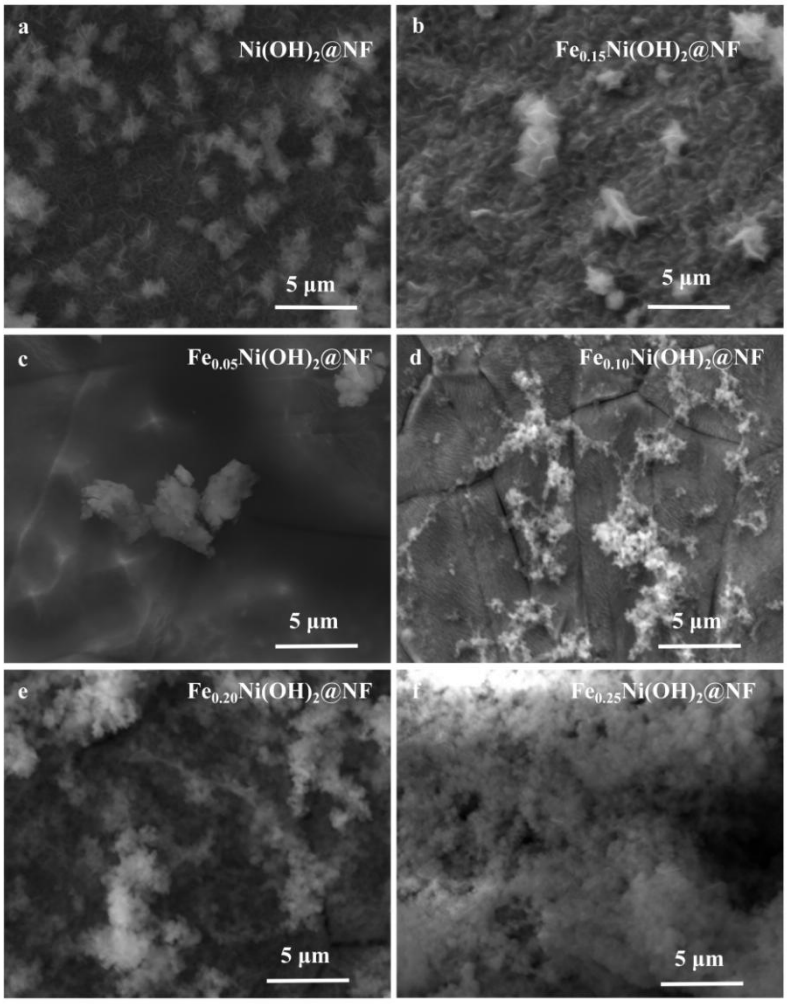

Fig. S2 SEM images of (a) $Ni(OH)_2$@NF, (b) $Fe_{0.15}Ni(OH)_2$@NF, (c) $Fe_{0.05}Ni(OH)_2$@NF, (d) $Fe_{0.10}Ni(OH)_2$@NF, (e) $Fe_{0.20}Ni(OH)_2$@NF and (f) $Fe_{0.25}Ni(OH)_2$@NF.

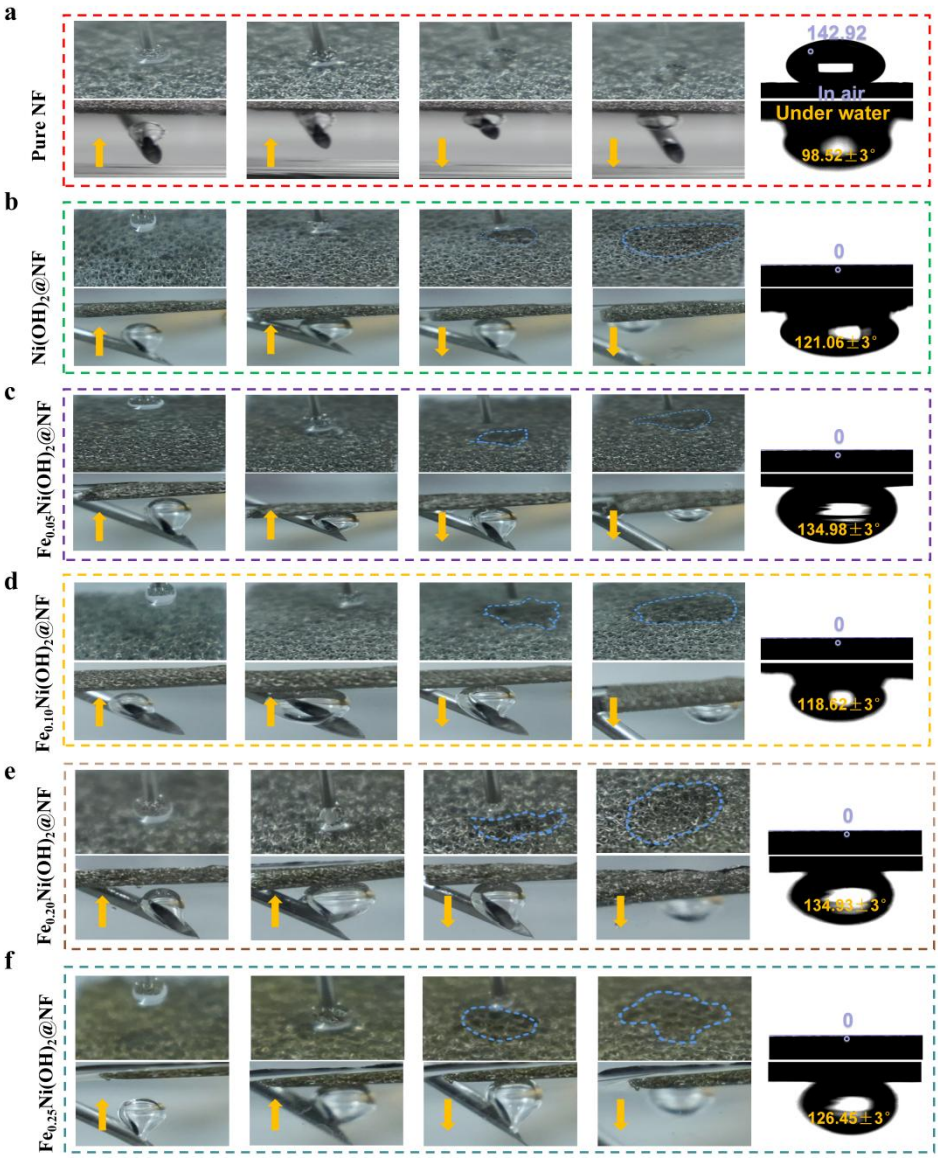

Fig. S3 Dynamic interfacial behaviors of droplets and bubbles of (a) NF, (b) $Ni(OH)_2$@NF, (c) $Fe_{0.05}Ni(OH)_2$@NF, (d) $Fe_{0.10}Ni(OH)_2$@NF, (e) $Fe_{0.20}Ni(OH)_2$@NF and (f) $Fe_{0.25}Ni(OH)_2$@NF.

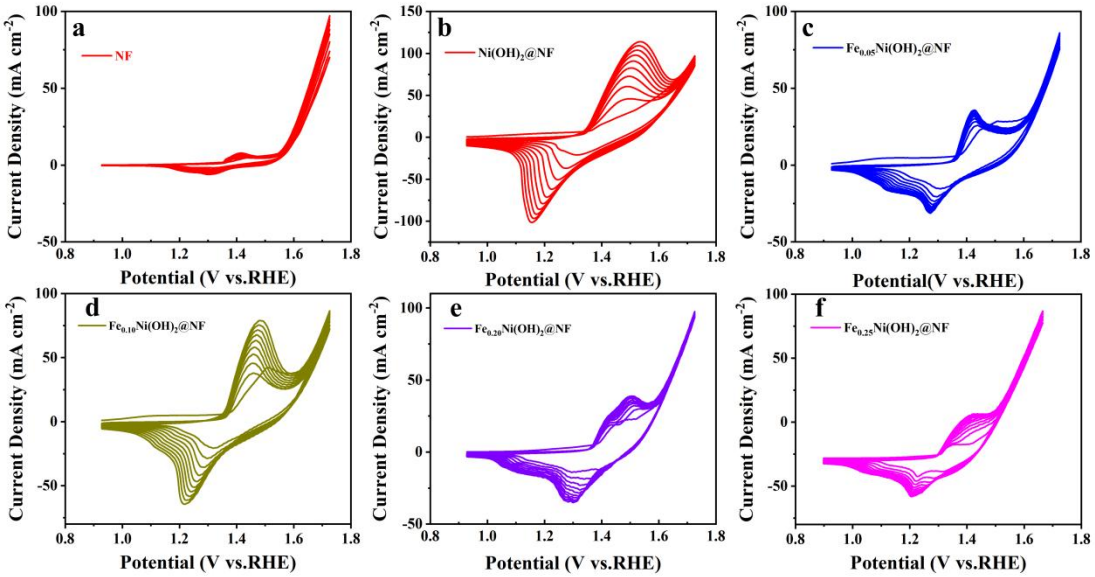

Fig. S4 CV curves of (a) NF, (b) $Ni(OH)_2$@NF, (c) $Fe_{0.05}Ni(OH)_2$@NF, (d) $Fe_{0.10}Ni(OH)_2$@NF, (e) $Fe_{0.20}Ni(OH)_2$@NF and (f) $Fe_{0.25}Ni(OH)_2$@NF in 1.0 M KOH.

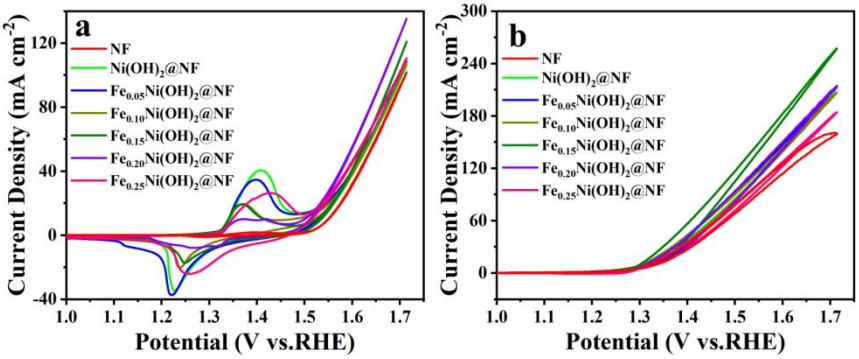

Fig. S5 CV curves of NF, $Ni(OH)_2$@NF and $Fe_XNi(OH)_2$@NF in a) 1.0 M KOH and b) 1.0 M KOH with 0.1 M glucose.

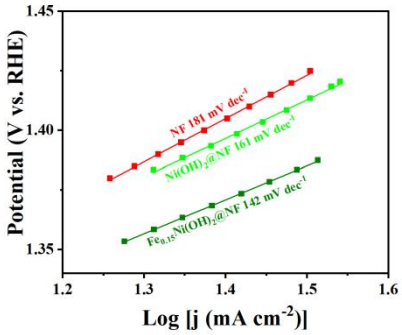

Fig. S6 Tafel slopes of NF, $Ni(OH)_2$@NF and $Fe_{0.15}Ni(OH)_2$@NF.

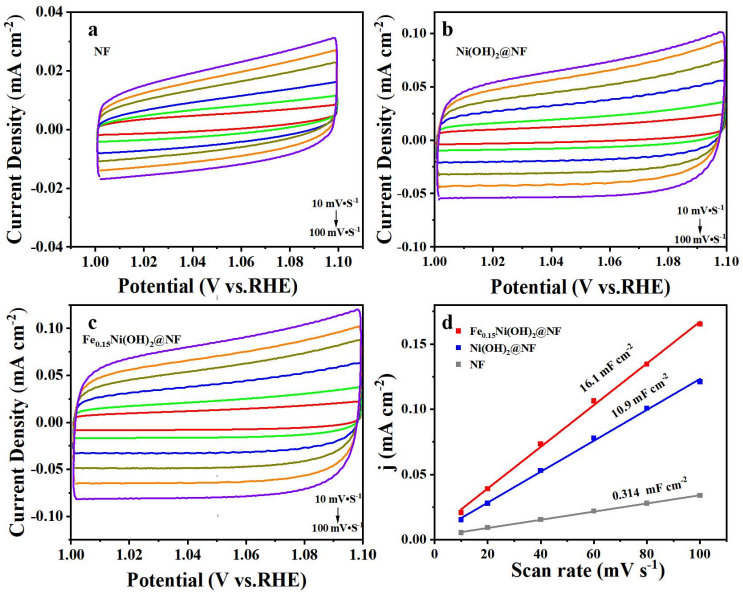

Fig. S7 CV curves in 1.0 M KOH with 0.1 M glucose of (a) NF, (b) $Ni(OH)_2$@NF, (c) $Fe_{0.15}Ni(OH)_2$@NF at various scan rates and corresponding d) capacitive current densities.

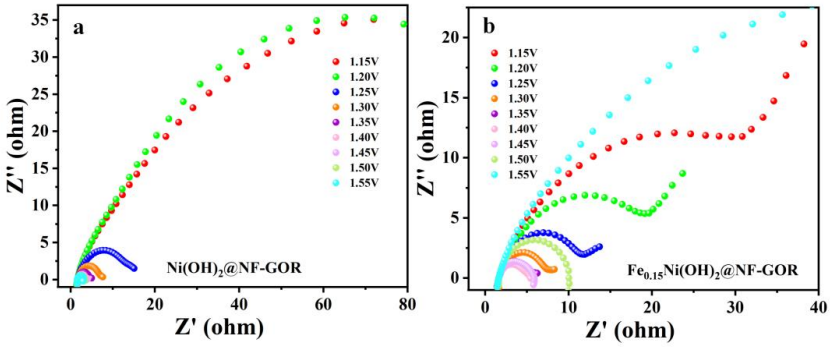

Fig. S8 Nyquist plots of (a) $Ni(OH)_2$@NF, (b) $Fe_{0.15}Ni(OH)_2$@NF for GOR.

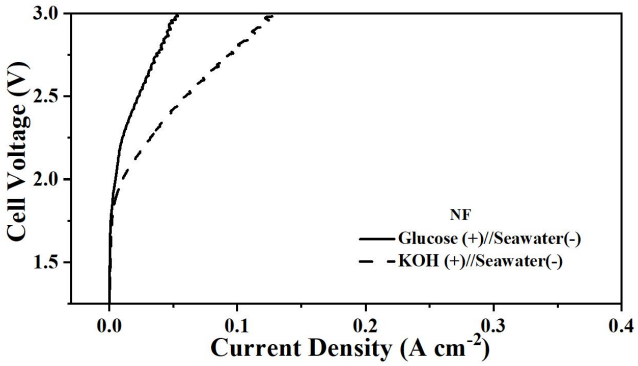

Fig. S9 Polarization curves for NF as anode and cathode under varying electrolyte conditions.

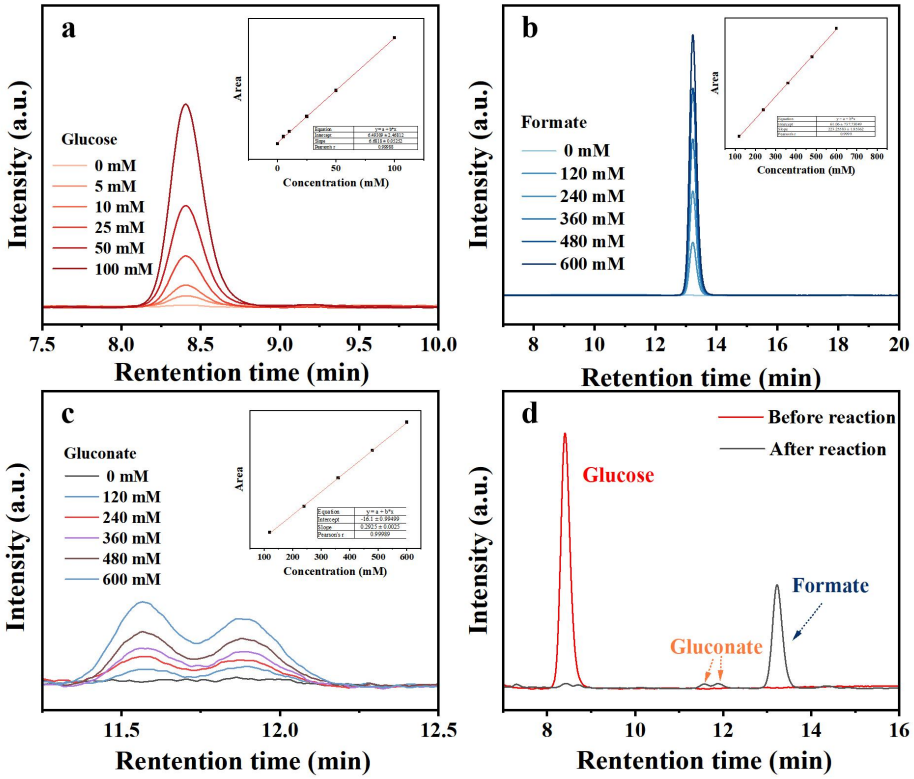

Fig. S10. HPLC measurements of pure (a) glucose, (b) formate and (c) gluconate. Inset display the calibration curves for each compound. (d) Comparative HPLC profiles of glucoes and oxidation products before and after chronopotentiometric measurements.

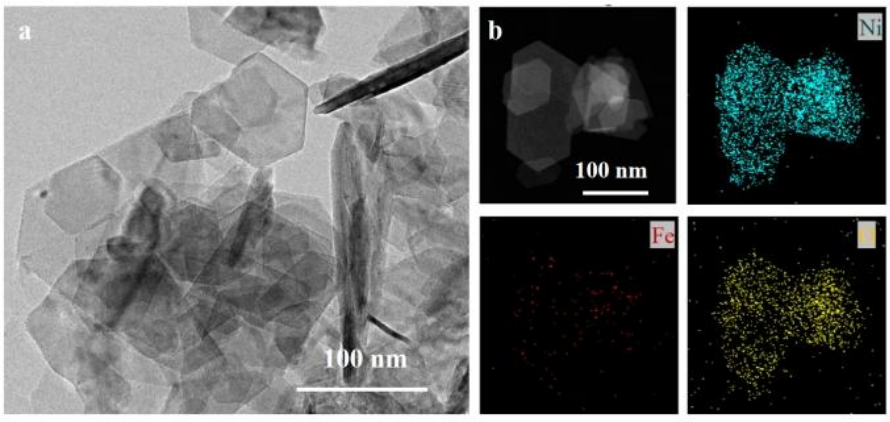

Fig. S11 TEM images and elemental mapping images of $Fe_{0.15}Ni(OH)_2$@NF after the 10 cycles test.

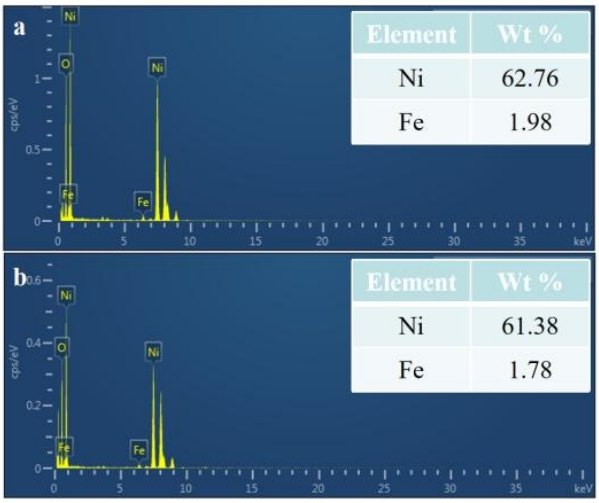

Fig. S12 EDS data of $Fe_{0.15}Ni(OH)_2$@NF (a) before and (b) after the 10 cycles test.

Table S1. The component element radio of Fe and Ni for $Fe_XNi(OH)_2$@NF according to the ICP-OES.

Sample	Fe content (ppb)	Ni content (ppb)	Fe/Ni	Amount of $Fe(NO_3)_3 \cdot 9H_2O$
$Ni(OH)_2$@NF	0	790.8	0	0 mmol
$Fe_{0.05}Ni(OH)_2$@NF	19.4	521.2	1/26.8	0.05 mmol
$Fe_{0.10}Ni(OH)_2$@NF	54.5	489.4	1/8.9	0.10 mmol
$Fe_{0.15}Ni(OH)_2$@NF	89.7	495.6	1/5.5	0.15 mmol
$Fe_{0.20}Ni(OH)_2$@NF	110.3	543.1	1/4.9	0.20 mmol
$Fe_{0.25}Ni(OH)_2$@NF	125.6	521.3	1/4.2	0.25 mmol

*Note that $Ni(OH)_2$@NF and $Fe_XNi(OH)_2$@NF were peeled off from Ni foam for ICP characterizations.

Table S2. Comparison of GOR performance for recently reported studies.

Electrocatalysts	Potential (V vs. RHE) @Current density (mA cm^{-2})	Glucose concentration (mM)	Ref.
$Fe_{0.15}Ni(OH)_2$@NF	1.38 @ 100	100	This work
$Cu(OH)_2$	1.49 @ 100	100	4
NiFeOx-NF	1.30 @87.6	100	7
Co_3FePx@NF	~ 1.24 @ 10	100	8
Co@NPC	1.46 @ 10	100	9
CoOOH	1.51 @ 100	100	6
NiVP/Pi-VC	1.27 @ 10	100	10
Ta-NiFe LDH	1.42 @ 50	100	11

Table S3. ICP-OES analysis of the total Fe and Ni in the electrolyte and $Fe_{0.15}Ni(OH)_2$@NF after the10 cycle test.

Element content*	Fe content (PPB)	Ni content (PPB)
$Fe_{0.15}Ni(OH)_2$@NF	78.3± 4.251	525.2 ± 10.721
Electrolyte	0.018 ± 0.011	0.625 ± 0.023

References

1 W. Zheng, *ACS Energy Letters*, 2023, 8, 1952–1958.

2 Y. J. Son, R. A. Marquez, K. Kawashima, L. A. Smith, C. E. Chukwuneke, J. Babauta and C. B. Mullins, *ACS Energy Letters*, 2023, 8, 4323–4329.

3 Y. Liang, Y. Li, H. Wang, J. Zhou, J. Wang, T. Regier and H. Dai, *Nature Materials*, 2011, 10, 780–786.

4 Y. Zhang, B. Zhou, Z. Wei, W. Zhou, D. Wang, J. Tian, T. Wang, S. Zhao, J. Liu, L. Tao, et al., *Advanced Materials*, 2021, 33, 2104791.

5 M. He, C. Huang, M. Sun, R. Wang, Y. Song, J. Su, W. Guo, Y. Xin, Q. Zhang, Y. Liu, et al., *Advanced Materials*, 2025, 38, 2419531.

6 Y. Q. Zhu, H. Zhou, J. Dong, S. M. Xu, M. Xu, L. Zheng, Q. Xu, L. Ma, Z. Li, M. Shao, et al., *Angewandte Chemie International Edition*, 2023, 62, e202219048.

7 W. J. Liu, Z. Xu, D. Zhao, X. Q. Pan, H. C. Li, X. Hu, Z. Y. Fan, W. K. Wang, G. H. Zhao, S. Jin, et al., *Nature Communications*, 2020, 11, 265.

8 J. Miao, X. Teng, R. Zhang, P. Guo, Y. Chen, X. Zhou, H. Wang, X. Sun and L. Zhang, *Applied Catalysis B: Environmental*, 2020, 263, 118109.

9 D. Li, Y. Huang, Z. Li, L. Zhong, C. Liu and X. Peng, *Chemical Engineering Journal*, 2022, 430, 132783.

10 N. Thakur, D. Mehta, A. Chaturvedi, D. Mandal and T. C. Nagaiah, *Journal of Materials Chemistry A*, 2023, 11, 13233–13244.

11 M. Tayebi, Z. Masoumi, B. Seo, C.-S. Lim, C. H. Hong, H. J. Kim, D. Kyung and H.-G. Kim, *ACS Applied Materials & Interfaces*, 2024, 16, 26107–26120.